Generation of continuous wave terahertz frequency radiation from MOCVD grown Fe-doped InGaAs and InGaAsP

Reshma A. Mohandas[1], Joshua R. Freeman[1,a] , Mark C. Rosamond[1], Osama Hatem[1,2], Siddhant Chowdhury[1], Lalitha Ponnampalam[3], Martyn Fice[3], Alwyn J. Seeds[3], Paul J. Cannard[4], Michael J. Robertson[4], David G. Moodie[4], John E. Cunningham[1], A Giles Davies[1], Edmund H. Linfield[1], and Paul Dean[1]

[1)] School of Electronic and Electrical Engineering, University of Leeds, Leeds LS2 9JT, United Kingdom.

[2)] Department of Engineering Physics, Faculty of Engineering, Tanta University, PO Box 31521, Egypt.

[3)] Department of Electronic and Electrical Engineering, University College London, London WC1E 6BT, United Kingdom

[4)] CIP Technologies, Adastral Park, Martlesham Heath, Ipswich, Suffolk IP5 3RE, United Kingdom

Abstract— We demonstrate the generation of continuous wave terahertz (THz) frequency radiation from photomixers fabricated on both Fe-doped InGaAs and Fe-doped InGaAsP, grown by metal-organic chemical vapor deposition. The photomixers were excited using a pair of distributed Bragg reflector (DBR) lasers with emission around 1550 nm, and THz radiation was emitted over a bandwidth of greater than 2.4 THz. Two InGaAs and four InGaAsP wafers with different Fe doping concentrations were investigated, with the InGaAs material found to outperform the InGaAsP in terms of emitted THz power. The dependencies of the emitted power on the photomixer applied bias, incident laser power, and material doping level, were also studied.

I. Introduction

There has been widespread interest in the applications of terahertz (THz) frequency technology across a range of fields including medical imaging,[1, 2] security screening,[3, 4] and non-destructive testing.[5] This interest has motivated the on-going development and improvement of THz imaging and spectroscopy systems in terms of their size, source power, spectral resolution and cost. Of the various methods available for the generation of THz radiation, photoconductive emission is arguably one of the most succesful owing to its room-temperature operation and high optical-to-electrical conversion efficiency.[6] Indeed, many implementations of THz imaging and spectroscopy systems exploit THz time-domain spectroscopy (THz-TDS) which is based on femtosecond excitation of photoconductive emitters and detectors; the resulting high signal-to-noise and large bandwidth (>2 THz) is well-suited to many applications. Despite these advantages, however, there are short-comings, which include a limited spectral resolution and a reliance on bulky and expensive femtosecond pulsed lasers.

An alternative approach to such time-domain methodologies is the use of photomixing, where CW THz radiation is generated by mixing two single-frequency lasers in a nonlinear medium; this is most easily and efficiently performed using a pair of diode lasers with a semiconductor surface acting as the nonlinear medium. The beating of the two laser fields produces sum and difference frequency components, the latter modulating the semiconductor conductance. Excited photocarriers are then accelerated under an applied electrical bias, which gives rise to the emission of THz radiation using a suitable antenna structure.[6] This approach is robust,[7] lends itself to compact integration, and also enables the use of widely-available and relatively inexpensive diode laser technologies. Furthermore, this generation scheme is widely tunable and produces narrowband emission with a linewidth derived

---

[a] Electronic mail: j.r.freeman@leeds.ac.uk

from the driving lasers, thereby allowing higher spectral resolution to be achieved compared to THz-TDS.[8-10]

The material that is most commonly used for THz photomixers is low-temperature-grown gallium arsenide (LT-GaAs)[11, 12] owing to its high resistivity and sub-picosecond carrier lifetimes. However, LT-GaAs has a bandgap corresponding to ~800 nm, which precludes the use of well-developed lasers, amplifiers, fibre optics and integrated components that operate in the telecommunications C-band (1530–1565 nm). This consideration has motivated the search for good quality photoconductive materials that can be driven at these wavelengths.[13] One of the most commonly used materials in this wavelength range is indium gallium arsenide (InGaAs), although the low resistivity of the intrinsic semiconductor makes it a poor choice for photoconductive emission. Over recent years several schemes to improve the characteristics of InGaAs for THz emission have been reported.[14-16] One method has been to incorporate Cr, Fe or group-V elements into the active InGaAs layer to create deep acceptor sites that act as scattering centres and compensate the intrinsic carrier concentration,[17] thereby increasing the material resistance. Earlier works based on this approach have reported pulsed THz emission from Fe-implanted InGaAs,[18] ion irradiated InGaAs,[19] Fe-doped InGaAs,[14, 20] and LT-InGaAs.[21] Similar materials have also been characterised for CW THz emission including ion irradiated InGaAs,[22] ion implanted InGaAs,[23] LT-InGaAs[24] and ErAs-InGaAs.[25]

An alternative material that can be used for CW THz emission at C-band is indium gallium arsenide phosphide (InGaAsP). When grown lattice-matched to indium phosphide (InP), the bandgap of InGaAsP corresponds to around 1300 nm.[26] Nevertheless, as shown in this work, the composition of this quaternary material can be engineered, and it is possible to produce high quality layers with absorption at 1550 nm. There have been two previous reports of THz photoconductive emission from InGaAsP under excitation from femtosecond lasers, namely using ion implanted material[27] and also the Fe-doped MOCVD material used in this work.[28] Similar to Fe-doped InGaAs, the Fe forms deep acceptors in the active layer, trapping the excess carriers and thus compensating the n-type nature of InGaAsP, and increasing the resistivity of the material. These trap sites are believed to act as mid-bandgap states capturing the photo-generated carriers.[15, 17]

In this work photomixers based on Fe-doped InGaAs and Fe-doped InGaAsP material, both grown by metal-organic vapour deposition (MOCVD), are investigated for CW THz emission for the first time. MOCVD ensures a better surface quality and more uniform doping compared to approaches such as ion irradiation.

The wafer structures used in this work are shown in Fig 1(a). The active InGaAs and InGaAsP layers were grown with the compositions Fe:$In_{0.53}Ga_{0.47}As$ and Fe:$In_{0.70}Ga_{0.30}As_{0.87}P_{0.13}$, respectively. For the case of Fe:InGaAsP, these molar fractions are expected to produce a bandgap close to 1550 nm,[26] which was confirmed experimentally by absorption spectroscopy. The MOCVD growth of InGaAs and InGaAsP layers was carried out on [100] InP substrates in a horizontal quartz reactor at a pressure of 810 torr and at growth temperature of 660° C. To ensure reproducibility for each growth, baking and cleaning of the susceptor and reactor were carried out. The precursors used were trimethylindium (TMI), trimethylgallium (TMG), 100% arsine (AsH_3) and 100% phosphine (PH_3) for the indium, gallium, arsenic and phosphorous atoms respectively. During the growth of the active layer, Fe:InGaAs or Fe:InGaAsP, the Fe was sourced from ferrocene ($Fe(C_5H_5)_2$) using a sublimation bubbler. Epitaxy was performed under a hydrogen environment with a flow rate of ~115 cm^3s^{-1}. The growth of the InGaAs and InGaAsP active layers was terminated with an n-InP layer to protect the As-rich layers during ex-situ annealing. The growth rates of the active layer and the InP buffer/cap layer were ~7.2 μm/hr and 3.00 μm/hr, respectively. The Fe doping of the active layer was carried out uniformly, allowing systematic control of the doping concentration for the different wafers. Following growth, the doping density of the different wafers was confirmed by secondary ion mass spectrometry (SIMS) analysis. It was observed that the surface quality of the Fe:InGaAsP wafers was significantly better than that of the ternary Fe:InGaAs wafers, for which FeAs precipitates formed notable defects, as can be seen in Fig 1(b). We attribute the improved surface of the quaternary material to better lattice matching with the InP substrate. The bandgaps of the materials were confirmed using photoluminescence (PL) measurements, which revealed emission peaks centred at ~1600 nm and ~1540 nm for Fe:InGaAs and Fe:InGaAsP wafers, respectively. [28]

Two InGaAs and four InGaAsP wafers of different Fe doping concentrations were investigated. The doping concentrations were 1×10^{16} cm^{-3}, 4×10^{16} cm^{-3}, 9.5×10^{16} cm^{-3} and 10×10^{16} cm^{-3} for the InGaAsP wafers, and 0.5×10^{16} cm^{-3} and 5.5×10^{16} cm^{-3} for the InGaAs wafers. Device fabrication started with the removal of the capping n-InP and n-InGaAs/n-InGaAsP layers. Concentrated hydrochloric acid was used to remove the n-InP layers whereas the n-InGaAs/n-InGaAsP layers were carefully removed using a calibrated sulphuric acid etch solution, exposing the Fe doped active layer. For larger electrode designs, n-InGaAs/n-InGaAsP layers can be used for defining contact electrodes,[29] but in this work the n-InGaAs/n-InGaAsP layer was removed and the contacts were defined directly on the active Fe doped layer. A three-turn self-complementary logarithmic spiral antenna with an active area of 11.3 µm × 11.3 µm was used throughout this study (Fig. 1(b)). The active region in the centre of the spiral contained three pairs of interdigitated fingers with a finger width of 0.2 µm and gaps of 1.6 µm. The antenna was patterned on each wafer by electron-beam lithography followed by Ti/Au metallization of 10 nm/150 nm. The contact pads were defined using Ti /Au (20 nm/100 nm).

As discussed previously, the aim of doping the material with Fe is to increase the resistivity of the intrinsic material. However, for the range of doping studied in this work, the resistivity was found to decrease with increased doping, suggesting that the material was over-compensated. Figure 2(a) shows the four-terminal resistivities of the two Fe:InGaAs wafers, which had values of ~1.0 kΩcm and ~ 0.6 kΩcm for the 0.5×10^{16} cm^{-3} and 5.5×10^{16} cm^{-3} doped samples, respectively. In the case of Fe:InGaAsP, the resistivity was found to decrease from ~10.0 kΩcm to ~1.0 kΩcm as the doping increased from 1×10^{16} cm^{-3} to 10×10^{16} cm^{-3}. This agrees with previous studies[15, 28, 30] where Fe-acceptors increase the resistivity from the measured intrinsic value of 1 kΩcm to a maximum at a doping of around 1×10^{16} cm^{-3}. The dark current of the devices studied in this work were of the order of ~5-10 µA at 0.2V applied bias for the lowest doped Fe:InGaAs and Fe:InGaAsP wafers.

Figure 2(b) shows the photo-resistance of the devices when illuminated with 10 mW of optical power at 1534 nm, measured at 0.2 V. The resistance of each device falls by almost three orders of magnitude under illumination. At this bias level, for the lowest doped Fe:InGaAs and Fe:InGaAsP wafers (with Fe doping concentrations of 0.5×10^{16} cm^{-3} and 1.0×10^{16} cm^{-3}, respectively), the photocurrents were ~ 2.5 mA. This reduced to ~1 mA and ~0.8 mA for the highest doped Fe:InGaAs and Fe:InGaAsP wafers, respectively (doping concentrations 5.5×10^{16} cm^{-3} and 10.0×10^{16} cm^{-3}). The lower photocurrents measured from the highly doped wafers are attributed to increased trapping of photo-carriers by Fe acceptors. For this measurement the DC bias was limited to 0.2 V to avoid thermal breakdown in the devices across the 1.6 µm gap, all devices showed ohmic behaviour in this range. We estimate a breakdown field in our devices of around ~12.5 kVcm^{-1}, based on dark current measurements. Much higher values are ~5×10^{2} kVcm^{-1} found in LT-GaAs,[31] but our values are comparable to those obtained in other work with ion implanted InGaAsP.[27]

The experimental apparatus used for characterization of the THz emission from the emitters is shown in Fig. 3. The devices were excited by a pair of commercially available, tunable fibre-coupled digital supermode distributed Bragg reflector lasers (Oclaro Lambda FLEX iTLA TL5000) operating in the telecommunications 'C-band' (1530–1565 nm). One laser (DBR1) was operated at a fixed wavelength while the other laser (DBR2) was electrically tuned, giving a software-limited frequency difference in the range of 0–2600 GHz. The outputs from the lasers were combined and then split using a 2 × 2 fibre splitter. An optical spectrum analyser was used to monitor the laser emission. The output from one fibre was collimated to free-space, passed through a half-wave plate and focused onto the emitter using an aspheric lens, providing 10 mW of incident optical power. The THz radiation generated from the emitter was then collimated using a 3.0-mm-diameter hyper-hemispherical silicon lens attached to the backside of the substrate and an f/2 parabolic mirror, and focussed to the detector using a second f/2 parabolic mirror. A commercial fibre-coupled InGaAs coherent receiver (TOPTICA Photonics InGaAs EK-000725) was employed as the detector, which was excited with 13 mW of optical power from the second output of the fibre splitter. The second parabolic mirror and detector were mounted on a computer-controlled mechanical delay line to enable phase control and ensure the optimum path difference between the emitter and detector arms of the system. The emitters were biased with square pulses at a frequency of 7.6 kHz and 1 V amplitude, and the detector signal was amplified using a trans-impedance amplifier with a gain of 10^7 Ω and monitored using a lock-in amplifier referenced to 7.6 kHz.

Figure 4 shows the THz signal amplitudes obtained from Fe:InGaAs and Fe:InGaAsP devices, plotted as a function of laser beat frequency. The emission bandwidths of the emitters were found to decrease with increasing doping over the doping range studied here. For example, the detectable signal bandwidth decreased from ~2.4 THz to ~2.0 THz in InGaAsP devices for an increase in doping from 1.0×10^{16} cm^{-3} to 10.0×10^{16} cm^{-3}. Likewise the measured bandwidth was ~2.4 THz and ~2.0 THz for the two Fe:InGaAs wafers with 0.5×10^{16} cm^{-3} and 5.5×10^{16} cm^{-3} doping, respectively. The sharp absorption features observed in the emission spectra correspond to atmospheric water absorption, as a result of the experiments being carried out in a non-purged environment. It should also be noted that the polarization of the radiation emitted from the log-spiral antenna is circular for the lower emission frequencies and becomes linear for the higher frequencies.[32] The detector used in this study couples to linearly polarised light, leading to a reduction in the signal detected at low radiation frequencies compared with a properly matched detector.

In the case of the Fe:InGaAsP emitters, the signal amplitude was found to be highest for the 4.0×10^{16} cm^{-3} doping concentration, although this level was similar to that obtained for the lowest doping sample (1.0×10^{16} cm^{-3}). Similarly, for Fe:InGaAs, the THz amplitude was greatest for the lowest doped wafer, (0.5×10^{16} cm^{-3}), in the doping range studied here. The improved performance from the lower doped wafers could be due to higher carrier mobility, as increasing the Fe doping is expected to cause higher carrier scattering, reducing the carrier mobility. This, in turn, will result in greater trapping of charge carriers by the Fe acceptors, leading to the observed decrease in signal amplitude with increased doping concentration. While there will be some benefit from having a reduced carrier lifetime, expected in the more highly doped samples, this appears not to be a dominant factor. The carrier mobility of the InGaAs wafers reported in previous works were in the range ~400–1000 cm^{2}V^{-1}s^{-1}.[15, 33]

By calibrating the experimental arrangement with a helium-cooled germanium bolometer, we estimate the average power after accounting for the 50% duty cycle from the low doped (0.5×10^{16} cm^{-3}) Fe:InGaAs emitter to be 45 nW at 1 THz, and ~6 nW at 2 THz. Similarly, for the Fe:InGaAsP emitter with doping 4.0×10^{16} cm^{-3}, the peak powers were 30 nW and ~6 nW at 1 THz and 2 THz, respectively. This slight difference in output powers between the Fe:InGaAs and Fe:InGaAsP is attributed to the difference in the material bandgaps resulting in lower optical absorption in the Fe:InGaAsP devices. These powers are higher than the previously reported 10 nW at 1 THz obtained from an InGaAs emitter with interdigitated fingers.[23] However, the reported power levels are still lower than a commercial InGaAs emitter (TOPTICA 10TB0027), which emits ~2 μW[b], ~300 nW and ~30 nW at 500 GHz, 1 THz and 2 THz respectively.

Figure 5 shows the roll-off in output power P_{THz} with frequency for the best performing Fe:InGaAs and Fe:InGaAsP devices, measured using the apparatus shown in Fig. 3 and corrected for the detector response with frequency by reference to the bolometer calibration. The measured roll-off is dominated by the carrier lifetime τ and the capacitance of the active region, C, as described by Eq.1, and can be used to estimate the value of τ,[34]

$$P_{THz}(\omega) \propto \frac{1}{2}\frac{(V_B G_0)^2 R_A}{\left[\left(1+(\omega\tau)^2\right)\left(1+(\omega R_A C)^2\right)\right]} \qquad (1)$$

The log-spiral antenna has radiation resistance of $R_A = 72\ \Omega$, and the capacitance of the fingers calculated from reference [34] is C = 2.5 fF. V_b is the bias applied to the emitter and G_0 is the dark conductance of the semiconductor. From Eq.1, the THz power is expected to exhibit a -12 dB/octave roll-off at high frequencies[32] owing to the carrier lifetime and RC time constant of the antenna. The Fe:InGaAs and Fe:InGaAsP emitters both have a roll-off of -6 dB/octave below 1100 GHz, caused by the carrier lifetime, which is estimated to be ~0.7-0.8 ps for both materials by fitting the experimental data to Eq. 1. The change to a -12 dB/octave roll-off above 1100 GHz is attributed to the extra contribution of the $R_A C$ time constant of the antenna. The 3 dB frequency calculated from this time constant is 880 GHz, which is consistent with the observed roll-off. It is interesting to note that the short carrier lifetimes measured for these wafers are inconsistent with the large DC photocurrent measured above; for the optical power used and the dimensions of the active area one would expect a significantly lower photocurrent. This could be partly explained by an underestimate of the power emitted at lower frequencies, due to poorer diffraction-limited coupling to the detector, causing an underestimation of the carrier lifetime. However, it is not possible to identify a single carrier lifetime that can explain both the large photocurrent and the power measured at high frequencies (see eqn. 1). This apparent discrepancy can be resolved, however, by the presence of two carrier lifetimes in the material. Indeed, as previously observed in pump-probe experiments on similar materials,[36] the presence of a finite number of trapping centres can result in a significant proportion of photogenerated carriers with a longer lifetime. While these carriers cannot contribute significantly to THz emission they can contribute to the photocurrent.

Figures 6(a) and (b) show the dependencies of THz power on applied bias and optical power, for the Fe:InGaAs (0.5×10^{16} cm^{-3}) and Fe:InGaAsP (4.0×10^{16} cm^{-3}) devices. For the bias dependence studies, a constant laser power of 10 mW was applied to the emitters. The THz power increased quadratically for all emitters as the 7.6 kHz square pulses were increased to a 1.25 V peak. No saturation of the THz signal was observed, suggesting that the carrier lifetime does not change in this bias range.[22] When the bias was increased beyond 1.25 V, corresponding to an applied field in the gap of ~7.8 kVcm^{-1}, the interdigitated fingers of the devices were damaged. This damage is thought to be caused by thermal breakdown, since it is below the estimated dielectric breakdown field of ~12.5 kVcm^{-1}. These

---

[b] The TOPTICA emitter was biased using square pulses of -2 V to 0.5 V amplitude at 7.6 kHz frequency at a laser power of 14 mW. For this emitter, the substrate is a heterostructure involving multiple periods rather than a single semiconductor layer.

breakdown fields are significantly lower than the field that can be applied to similar LT-GaAs devices, owing to the lower resistivities in InGaAs and InGaAsP.

Figure 6(b) shows the variation of emitted THz power with optical laser power. In this case the emitters were biased using square pulses of amplitude 1 V and an erbium-doped fibre amplifier provided optical powers up to 20 mW. The detector excitation was kept at constant optical power of 13 mW and the measured THz power was calculated by comparison with a calibrated device. Saturation of the emitted THz power is observed as the optical power is increased, due to the screening of the applied bias by the photo-generated carriers.

In summary, a range of Fe-doped InGaAs and InGaAsP wafers, grown by MOCVD with doping levels in the range 0.5×10^{16} cm^{-3} to 10×10^{16} cm^{-3}, have been assessed for use in photoconductors for CW THz emission. The devices produced emission bandwidths up to 2.4 THz for both InGaAs and InGaAsP, with doping concentrations of 0.5×10^{16} cm^{-3} and 4.0×10^{16} cm^{-3}, respectively. It was found that devices with lower doping performed better for both InGaAs and InGaAsP in the doping range studied here, suggesting over-compensation by Fe-doping. Smaller signal amplitudes were observed for InGaAsP devices compared to InGaAs devices with similar doping concentrations, despite the higher surface quality of Fe:InGaAsP.

The results presented here demonstrate that high-performance systems based on CW THz generation and detection in photomixers can be accomplished using reproducible MOCVD grown material, commercial DBR lasers in the telecommunications ‘C-band’, simple fabrication techniques and simple driving electronics.

ACKNOWLEDGEMENTS

This work was supported by the Engineering and Physical Sciences Research Council [EP/J017671/1, ‘COTS’ and EP/J002356/1]. Funding was also received from the European Community’s Seventh Framework Programme [FP7-IDEAS-ERC] under grant agreement number 247375 ‘TOSCA’. Support from the Royal Society and Wolfson Foundation (AGD and EHL) is also acknowledged. The data associated with this paper are openly available from the University of Leeds data repository.[37]

REFERENCES

[1] T. Ouchi, K. Kajiki, T. Koizumi, T. Itsuji, Y. Koyama, R. Sekiguchi, O. Kubota, and K. Kawase, Journal of Infrared, Millimeter, and Terahertz Waves **35**, 118 (2014).

[2] V. P. Wallace, A. J. Fitzgerald, S. Shankar, N. Flanagan, R. Pye, J. Cluff, and D. D. Arnone, British Journal of Dermatology **151**, 424 (2004).

[3] N. Karpowicz, H. Zhong, C. Zhang, K.-I. Lin, J.-S. Hwang, J. Xu, and X. C. Zhang, Applied Physics Letters **86**, 054105 (2005).

[4] A. G. Davies, A. D. Burnett, W. Fan, E. H. Linfield, and J. E. Cunningham, Materials Today **11**, 18 (2008).

[5] J. A. Zeitler and Y.-C. Shen, in Terahertz Spectroscopy and Imaging, edited by K.-E. Peiponen, A. Zeitler and M. Kuwata-Gonokami (Springer Berlin Heidelberg, 2013), Vol. 171, p. 451.

[6] S. Preu, G. H. Dohler, S. Malzer, L. J. Wang, and A. C. Gossard, Journal of Applied Physics **109**, 061301 (2011).

[7] J. E. Bjarnason, T. L. J. Chan, A. W. M. Lee, E. R. Brown, D. C. Driscoll, M. Hanson, A. C. Gossard, and R. E. Muller, Applied Physics Letters **85**, 3983 (2004).

[8] K. Nicholas, Z. Hua, X. Jingzhou, I. L. Kuang, H. Jenn-Shyong, and X. C. Zhang, Semiconductor Science and Technology **20**, S293 (2005).

9 M. Usami, T. Iwamoto, R. Fukasawa, M. Tani, M. Watanabe, and K. Sakai, Physics in Medicine and Biology **47**, 3749 (2002).

10 F. F. John, S. Brian, H. Feng, G. Dale, B. Robert, O. Filipe, and Z. David, Semiconductor Science and Technology **20**, S266 (2005).

11 E. R. Brown, K. A. McIntosh, K. B. Nichols, and C. L. Dennis, Applied Physics Letters **66**, 285 (1995).

12 S. Matsuura, M. Tani, and K. Sakai, Applied Physics Letters **70**, 559 (1997).

13 G. Keiser, in Wiley Encyclopedia of Telecommunications (John Wiley & Sons, Inc., 2003).

14 S. Sengupta, I. Wilke, and P. S. Dutta, Applied Physics Letters **95** (2009).

15 B. Tell, U. Koren, and B. I. Miller, Journal of Applied Physics **61**, 1172 (1987).

16 C. Carmody, H. H. Tan, C. Jagadish, A. Gaarder, and S. Marcinkevicius, Applied Physics Letters **82**, 3913 (2003).

17 S. M. Gulwadi, M. V. Rao, A. K. Berry, D. S. Simons, P. H. Chi, and H. B. Dietrich, Journal of Applied Physics **69**, 4222 (1991).

18 M. Suzuki, M. Tonouchi, and K.-i. Fujii, in Infrared and Millimeter Waves and 13th International Conference on Terahertz Electronics, 2005. IRMMW-THz 2005. The Joint 30th International Conference on, 2005), p. 251.

19 J. Mangeney and P. Crozat, Comptes Rendus Physique **9**, 142 (2008).

20 C. D. Wood, O. Hatem, J. E. Cunningham, E. H. Linfield, A. G. Davies, P. J. Cannard, M. J. Robertson, and D. G. Moodie, Applied Physics Letters **96**, 194104 (2010).

21 R. Wilk, M. Mikulics, K. Biermann, H. Künzel, I. Z. Kozma, R. Holzwarth, B. Sartorius, M. Mei, and M. Koch, in Conference on Lasers and Electro-Optics/Quantum Electronics and Laser Science Conference and Photonic Applications Systems Technologies (Optical Society of America, Baltimore, Maryland, 2007), p. CThR2.

22 N. Chimot, J. Mangeney, P. Crozat, J. Lourtioz, K. Blary, J. Lampin, G. Mouret, D. Bigourd, and E. Fertein, Opt. Express **14**, 1856 (2006).

23 J. Mangeney, A. Merigault, N. Zerounian, P. Crozat, K. Blary, and J. F. Lampin, Applied Physics Letters **91**, 241102 (2007).

24 C. Baker, I. Gregory, M. Evans, W. Tribe, E. Linfield, and M. Missous, Opt. Express **13**, 9639 (2005).

25 C. W. Berry, M. R. Hashemi, S. Preu, H. Lu, A. C. Gossard, and M. Jarrahi, Applied Physics Letters **105** (2014).

26 M. Silver and E. P. O'Reilly, Quantum Electronics, IEEE Journal of **31**, 1193 (1995).

27 A. Fekecs, M. Bernier, D. Morris, M. Chicoine, F. Schiettekatte, P. Charette, and R. Arès, Opt. Mater. Express **1**, 1165 (2011).

28 O. Hatem, J. R. Freeman, J. E. Cunningham, P. J. Cannard, M. J. Robertson, E. H. Linfield, A. G. Davies, and D. G. Moodie, Journal of Infrared, Millimeter, and Terahertz Waves, 1 (2015).

29 O. Hatem, J. Cunningham, E. H. Linfield, C. D. Wood, A. G. Davies, P. J. Cannard, M. J. Robertson, and D. G. Moodie, Applied Physics Letters **98**, 121107 (2011).

30 A. R. Clawson, D. P. Mullin, D. I. Elder, and H. H. Wieder, Journal of Crystal Growth **64**, 90 (1983).

31 S. Verghese, K. A. McIntosh, and E. R. Brown, Microwave Theory and Techniques, IEEE Transactions on **45**, 1301 (1997).

32 I. S. Gregory, C. Baker, W. R. Tribe, I. V. Bradley, M. J. Evans, E. H. Linfield, G. Davies, and M. Missous, Quantum Electronics, IEEE Journal of **41**, 717 (2005).

33 M. Martin and E. R. Brown, in Proc. SPIE 8261 Terahertz Technology and Applications V, 2012), p. 826102.

34 E. R. Brown, F. W. Smith, and K. A. McIntosh, Journal of Applied Physics **73**, 1480 (1993).

35 J. B. D. Soole and H. Schumacher, Electron Devices, IEEE Transactions on **37**, 2285 (1990).

36 A. K. Azad, R. P. Prasankumar, D. Talbayev, A. J. Taylor, R. D. Averitt, J. M. O. Zide, H. Lu, A. C. Gossard, and J. F. O'Hara, Applied Physics Letters **93**, 121108 (2008).

37 http://doi.org/10.5518/22.

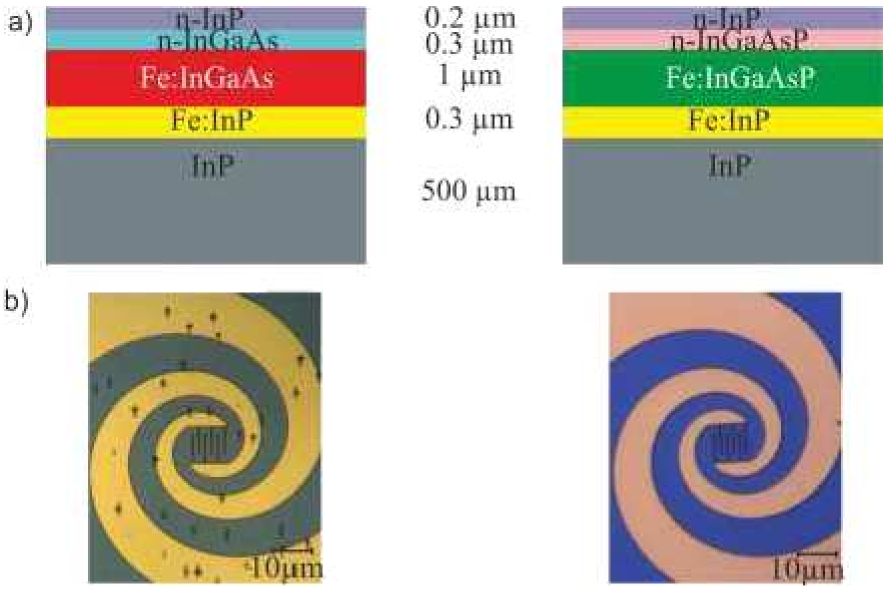

FIG 1: (a) Layer structure and thicknesses of the Fe:InGaAs and Fe:InGaAsP wafers grown on InP substrate by MOCVD. (b) Fabricated log-spiral antennas on Fe:InGaAs and Fe:InGaAsP wafers with interdigitated fingers in the active region. FeAs precipitates are visible on the InGaAs surface.

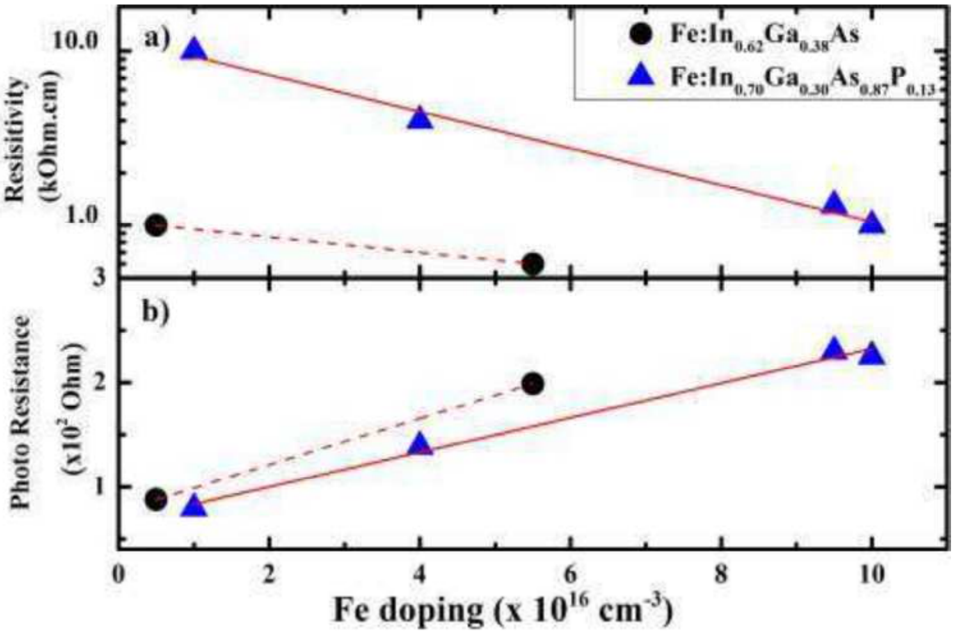

FIG 2: (a) Resistivity, measured under dark conditions, and (b) emitter photo-resistance, as a function of Fe doping for InGaAs and InGaAsP material. Lines are guides for the eye.

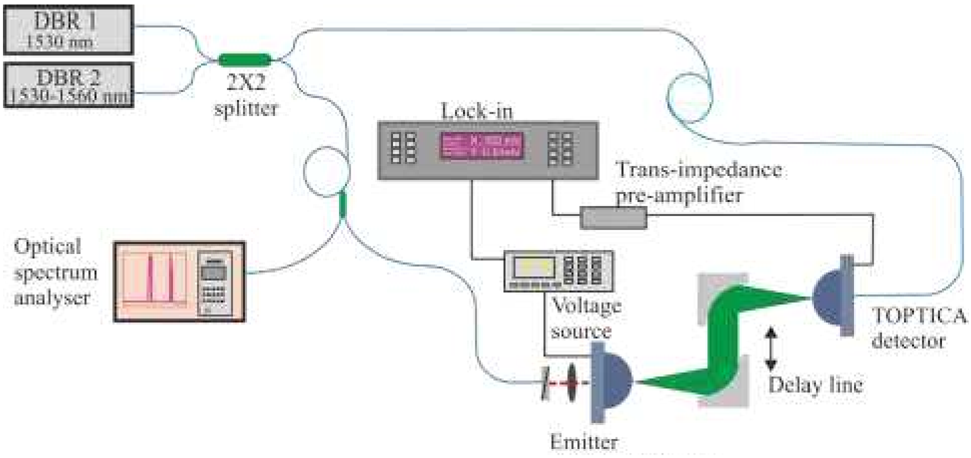

FIG 3: Experimental arrangement for emitter characterization.

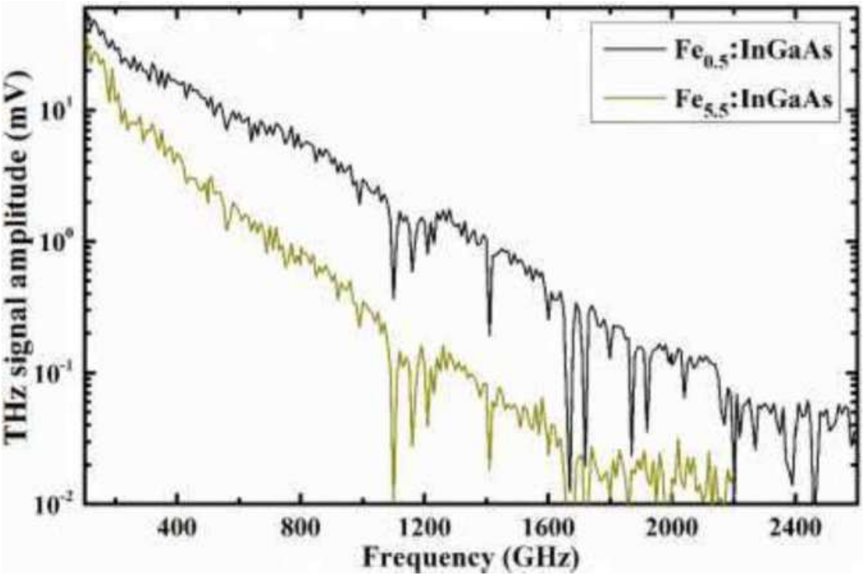

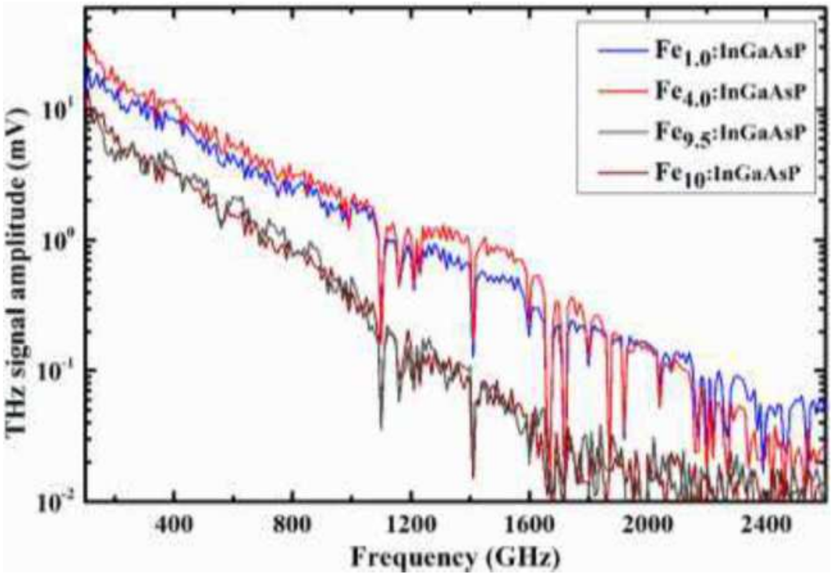

FIG 4: Measured THz peak field as a function of heterodyne frequency for Fe:InGaAs and Fe:InGaAsP with different doping concentrations. Sharp features in the curves correspond to the water absorption lines are visible to above 2.4THz.

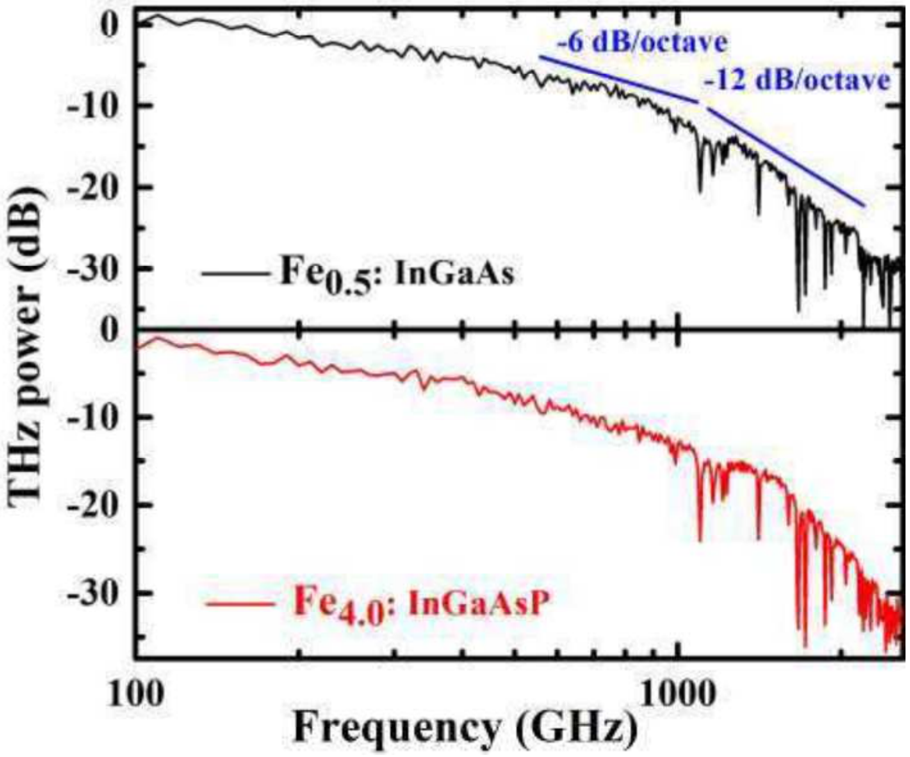

FIG 5: THz power as a function of heterodyne frequency for Fe:InGaAs and Fe:InGaAsP wafers with (top) $0.5\times10^{16}\,cm^{-3}$ and (bottom) $4.0\times10^{16}\,cm^{-3}$ Fe doping concentrations.

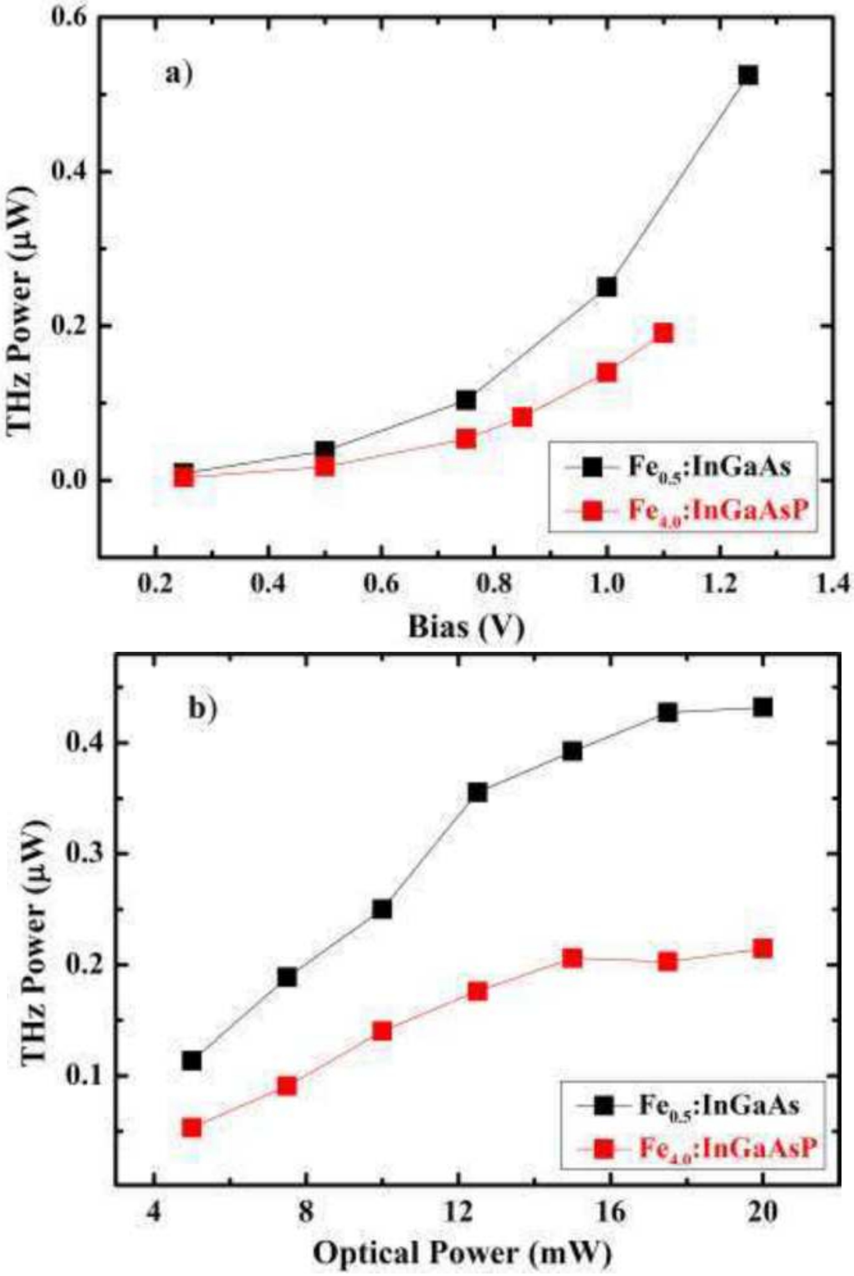

FIG 6: THz power as a function of (a) bias and (b) optical power at 500 GHz for $Fe_{0.5}$:InGaAs and $Fe_{4.0}$:InGaAsP